Sanin V.N., Ikornikov D.M., and etc. Synthesis of refractory high-entropy alloys based ...



Self-Propagating High-Temperature Synthesis Самораспространяющийся высокотемпературный синтез



UDC 621.762

https://doi.org/10.17073/1997-308X-2025-5-17-35

Research article Научная статья



Synthesis of refractory high-entropy alloys based on Mo-Nb-Ta-(Cr, V, Zr, Hf) using centrifugal SHS metallurgy and investigation of their oxidation resistance

V. N. Sanin¹, D. M. Ikornikov¹ , A. O. Sivakova¹, D. Yu. Kovalev¹, S. L. Silyakov¹, M. D. Panova²

Merzhanov Institute of Structural Macrokinetics and Materials Science of the Russian Academy of Sciences
 8 Academician Osip'yan Str., Chernogolovka, Moscow Region 142432, Russia

 JSC "State Scientific Research and Design Institute of the Rare Metal Industry "Giredmet"
 2 Elektrodnaya Str., Moscow 111524, Russia

denis-ikornikov@yandex.ru

Abstract. Refractory high-entropy alloys (RHEAs) based on refractory metals exhibit a combination of outstanding properties, such as high strength and thermal stability at elevated temperatures. These alloys typically contain costly refractory elements, including Mo. Nb. Ta. W. and Hf. In addition to their high cost, RHEA production is associated with a number of technological challenges. Well-established commercial methods used for nickel-based superalloys are generally unsuitable due to the higher melting points and increased chemical reactivity of the components. To address this issue, the present study explores the feasibility of synthesizing cast RHEAs using centrifugal self-propagating high-temperature synthesis (SHS) metallurgy - a technological approach within the broader field of SHS. For the first time, cast RHEAs based on the Mo-Nb-Ta system, alloyed in situ with 3d metals (Cr, V, Zr, Hf), were successfully synthesized via SHS. It was demonstrated that crystallization of the ingots occurs from the molten state, ensuring homogeneous distribution of Mo, Nb, Ta, Cr, V, Zr, and Hf. The phase composition of the synthesized RHEAs was found to depend on the alloying elements. Co-reduction of group V (Nb, Ta, V) and group VI (Cr, Mo) metals resulted in nearly single-phase alloys with a body-centered cubic (BCC) structure typical for these elements. The addition of Zr and Hf - metals with a hexagonal crystal structure - to the quaternary MoNbTaCr alloy significantly altered the phase composition of the ingots. In addition to BCC-phase reflections, the X-ray diffraction patterns exhibited intense reflections of facecentered cubic (FCC) phases and weak reflections of two hexagonal close-packed (HCP) phases. The proposed synthesis method considerably simplifies the otherwise complex technological process of producing cast, multicomponent RHEAs with a desired composition. Oxidation resistance tests revealed that the Mo-Nb-Ta-Cr-V composition is the most promising for further investigation. Compared to other compositions, this alloy demonstrated superior oxidation resistance, making it a competitive candidate for high-temperature applications.

Keywords: self-propagating high-temperature synthesis (SHS); centrifugal SHS metallurgy; thermite-type SHS systems; high-entropy alloys (HEAs); refractory high-entropy alloys (RHEAs); multimetallic alloy synthesis; oxidation resistance of HEAs

Acknowledgements: The research was supported by the Russian Science Foundation (Project No. 24-13-00065, https://rscf.ru/project/24-13-00065/

For citation: Sanin V.N., Ikornikov D.M., Sivakova A.O., Kovalev D.Yu., Silyakov S.L., Panova M.D. Synthesis of refractory high-entropy alloys based on Mo–Nb–Ta–(Cr, V, Zr, Hf) using centrifugal SHS metallurgy and investigation of their oxidation resistance. Powder Metallurgy and Functional Coatings. 2025;19(5):17–35. https://doi.org/10.17073/1997-308X-2025-5-17-35



Синтез высокоэнтропийных сплавов на основе тугоплавких металлов Mo-Nb-Ta-(Cr, V, Zr, Hf) методами центробежной СВС-металлургии и исследование их окислительной стойкости

В. Н. Санин¹, Д. М. Икорников¹, А. О. Сивакова¹, Д. Ю. Ковалев¹, С. Л. Силяков¹, М. Д. Панова²

¹ Институт структурной макрокинетики и проблем материаловедения им. А.Г. Мержанова РАН Россия, 142432, Московская обл., г. Черноголовка, ул. Академика Осипьяна, 8 ² АО «Государственный научно-исследовательский и проектный институт редкометаллической промышленности «Гиредмед» Россия, 111524, г. Москва, ул. Электродная, 2

■ denis-ikornikov@yandex.ru

Аннотация. Высокоэнтропийные сплавы на основе тугоплавких металлов (ТВЭС) (англ. RHEAs – refractory high-entropy alloys) обладают набором замечательных свойств – такими, как высокая прочность и термическая стабильность при высоких температурах. В состав этих сплавов входит ряд дорогостоящих тугоплавких элементов: Мо, Nb, Ta, W, Hf и др. Помимо высокой стоимости, получение ТВЭС характеризуется рядом технологических трудностей. Успешно действующие коммерческие технологии для никелевых жаропрочных сплавов здесь практически не применимы вследствие более высоких температур плавления компонентов и их высокой химической активности. Для решения этой проблемы в настоящей работе исследована возможность получения литых ТВЭС методом центробежной СВС-металлургии – одним из технологических направлений в области самораспространяющегося высокотемпературного синтеза (СВС). Используя данный метод, впервые были получены литые ТВЭС на основе базовой системы, состоящей из тугоплавких металлов Mo–Nb–Ta, легированные 3*d*-металлами (Cr, V, Zr, Hf) непосредственно (in situ) путем СВС. Показано, что кристаллизация слитков происходит из жидкого состояния, в котором обеспечивается гомогенное распределение элементов Mo-Nb-Ta-(Cr, V, Zr, Hf). Выявлено, что фазовый состав синтезируемых слитков ТВЭС зависит от сплавляемых компонентов. При совместном восстановлении металлов V (Nb, Ta, V) и VI (Cr, Mo) групп формируются практически однофазные сплавы, имеющие кристаллическую структуру ОЦК, характерную для металлов этих групп. Введение в 4-компонентный сплав MoNbTaCr элементов Zr и Hf, имеющих гексагональную кристаллическую структуру, приводит к существенному изменению фазового состава слитков с рефлексами ОЦК-фазы на дифрактограмме, где присутствуют интенсивные рефлексы ГЦК-фазы, а также слабые рефлексы двух ГПУ-фаз. Показано, что применение предлагаемого метода существенно упрощает сложную технологическую задачу по получению литых многокомпонентных ТВЭС заданного состава. Изучением окислительной стойкости полученных материалов установлено, что состав Mo-Nb-Ta-Cr-V наиболее перспективен для дальнейшего исследования и, в сравнении с другими составами, имеет хорошие показатели по жаростойкости, что делает данный материал конкурентоспособным для высокотемпературного использования.

Ключевые слова: самораспространяющийся высокотемпературный синтез (СВС), центробежная СВС-металлургия, СВС-системы термитного типа, высокоэнтропийные сплавы (ВЭС), сплавы на основе тугоплавких металлов, получение полиметаллических сплавов, окислительная стойкость ВЭС

Благодарности: Работа выполнена за счет гранта Российского научного фонда № 24-13-00065, https://rscf.ru/project/24-13-00065/

Для цитирования: Санин В.Н., Икорников Д.М., Сивакова А.О., Ковалев Д.Ю., Силяков С.Л., Панова М.Д. Синтез высокоэнтропийных сплавов на основе тугоплавких металлов Мо–Nb–Ta–(Cr, V, Zr, Hf) методами центробежной СВС-металлургии и исследование их окислительной стойкости. *Известия вузов. Порошковая металлургия и функциональные покрытия*. 2025;19(5):17–35. https://doi.org/10.17073/1997-308X-2025-5-17-35

Introduction

Since the first studies published in 2004 [1; 2], a new paradigm based on multicomponent alloy design has been introduced into materials science, laying the foundation for the development of a novel class of metallic materials. These materials, referred to as high-entropy alloys (HEAs), have remained the focus of intense research interest over the past two decades.

In addition to their multicomponent nature, a defining feature of HEAs is their tendency to form predominantly single-phase, thermodynamically stable, disordered substitutional solid solutions with high-symmetry crystal lattices – typically face-centered cubic (FCC) or body-centered cubic (BCC) [3–6].

Initial investigations proposed that the high configurational entropy of mixing, arising from the pre-



sence of multiple principal elements in equiatomic or near-equiatomic ratios, would favor the formation of disordered solid solutions over ordered intermetallic phases. As a result, these high-entropy solid solutions were expected to simultaneously exhibit high strength and sufficient ductility. However, subsequent studies revealed that entropy alone is not always the dominant factor governing the formation of disordered solid solutions in real alloy systems. It has since been established that the phase composition of HEAs is determined primarily by the specific atomic properties of the constituent elements rather than their number [7–12].

It is anticipated that HEAs will surpass the performance of conventional commercial structural alloys [13–16] owing to rational composition design (including deviations from strict equiatomicity) and the development of advanced microstructural control tools, such as novel synthesis techniques and post-processing via thermal or mechanical treatments. Numerous HEAs have already been identified that exhibit superior physicochemical properties compared to traditional alloys [4; 7; 11–17].

Among the various families of HEAs [18], a special place is held by refractory high-entropy alloys (RHEAs), which are designed for high-temperature service and are composed mainly of high-melting-point elements such as niobium (Nb), molybdenum (Mo), tantalum (Ta), tungsten (W), rhenium (Re), and hafnium (Hf) [14; 18–23]. Refractory metals are known for their high strength and resistance to deformation at elevated temperatures, making them ideal candidates for the development of RHEAs.

Early studies [22; 23] reported that BCC-structured RHEAs such as NbMoTaW and VNbMoTaW demonstrate good strengthening behavior at room temperature and structural stability up to 1400 °C. Remarkably, these alloys retained yield strengths of 405 and 477 MPa, respectively, even at 1600 °C, clearly indicating their promising potential for practical high-temperature applications. As a result, RHEAs are being actively explored for use in the aerospace and aviation industries, particularly for components in high-temperature gas turbine systems where there is a demand to increase operating temperatures beyond the limits of current nickel-based superalloys (up to 1100 °C) [24; 25].

The main drawbacks of the earliest RHEAs – based on refractory elements such as Mo, Nb, Ta, W, and V – were their very high density and low oxidation resistance [23]. To address these issues, subsequent efforts focused on substituting or partially replacing these elements with lighter and more accessible ones, such as Cr, Ti, Zr, Co, Mn, and Al [18; 26–38]. The incorporation of such elements improves specific strength, oxida-

tion and corrosion resistance, thermal shock resistance, creep resistance, and high-temperature deformation behavior. Most RHEA studies to date have focused on understanding structure—property relationships, while comparatively little attention has been paid to developing new, effective synthesis methods that offer precise control over alloy composition and the designed distribution of structural constituents.

At the same time, expanding the range of elements used in RHEA design introduces significant technological challenges. These stem from the extremely high melting points of key components (e.g., W, Mo, Nb, Re, Hf), the large differences in melting temperatures between base and alloying elements (e.g., Al, Ti, V, Cr, Fe), and the high chemical reactivity of certain constituent elements, as well as other factors.

Numerous laboratory-scale methods have been proposed currently for RHEA synthesis [18; 38], including mechanochemical approaches (mechanical alloying, MA), combinations of MA with spark plasma sintering (SPS), electrochemical techniques [39], additive 3D manufacturing, and melting-based metallurgical processes. However, most of these methods share common drawbacks: the requirement for high-purity elemental feedstock, high energy consumption, and low productivity – factors that are acceptable for research purposes but not for industrial-scale production (with the exception of melting techniques). Among all available methods, casting remains the most promising for producing RHEAs [18; 38]. The most common techniques include vacuum arc remelting (VAR), vacuum induction melting (VIM), and, less frequently, electron beam melting (EBM). However, melting modes suitable for conventional alloys are inadequate for RHEAs. The presence of refractory elements (W, Mo, Ta, Nb, Hf) demands significantly higher temperatures and extended holding times in the molten state to ensure full intermixing and dissolution. To avoid elemental segregation and macrosegregation, multiple melting cycles (up to 5–6) are typically required. Furthermore, RHEAs produced via VAR often have relatively coarse grain structures (ranging from 100 to 300 µm), which limits the grain boundary strengthening effect.

We previously demonstrated the feasibility of synthesizing cast HEAs based on 3d metals (Co–Cr–Fe–Ni–Mn) using centrifugal SHS metallurgy [40; 41] – a direction within the broader, energy-efficient class of self-propagating high-temperature synthesis (SHS) technologies. Subsequently, *in situ* SHS was used to produce composite materials based on these HEAs, incorporating strengthening structural precipitates such as $Mo(Nb)_5SiB_2$, $Mo(Nb)_3Si$, and $MoSi_2$ [42].



The aim of the present study was to investigate the possibility of synthesizing cast RHEAs based on the Mo-Nb-Ta system alloyed with 3d metals (Cr, V, Zr, Hf, Ti) using centrifugal SHS metallurgy and to examine the influence of the alloying system on a key performance characteristic – oxidation resistance.

The ability to produce cast RHEAs without furnace equipment and high energy input offers significant potential for practical applications. SHS metallurgy relies on oxide raw materials (metal oxides) and the chemical energy released during highly exothermic reactions initiated in a combustion front through a compacted powder charge. The SHS process requires no external energy input. This approach may prove substantially more cost-effective than traditional melting of pure metals. Moreover, the high synthesis temperature (above 2300 °C) and the action of centrifugal forces (g-forces) enable enhanced dissolution of alloying components, improved metal reduction completeness, and more efficient separation of metallic and oxide phases [40–44].

1. Starting powder components and experimental scheme for RHEA synthesis

As previously demonstrated [40–44], the use of highly exothermic thermite-type SHS mixtures makes it possible to reach temperatures sufficient for producing reaction products in the molten state (above 2500 °C), and thereby obtain the synthesized material in a cast form, including cast HEAs [40–42].

The synthesis was carried out using thermite-type SHS systems containing powder oxides of the target elements (MoO₃, Nb₂O₅, Ta₂O₅, Cr₂O₃, V₂O₅, TiO₂), Zr–Mo and Hf–Mo master alloys, a metallic reducing agent (Al), and functional additives (fluxing agents CaO and CaF₂). Selected characteristics of the primary powder reagents used are listed in Table 1.

All starting oxide powders were pre-dried to remove adsorbed moisture in SNOL-type drying ovens (t = 90 °C, $\tau = 1$ h). After weighing the components (calculated to achieve the target alloy composition), the reagents were mixed in an MP4/5.0 planetary mill with a drum volume of up to 5 L for 15–20 min at a ball-to-charge mass ratio of 1:10. The elements Zr and Hf were introduced into the reaction mixture in the form of Zr–Mo and Hf–Mo master alloys, custom-fabricated for this purpose.

The charge composition was determined based on the stoichiometry of the following main reactions:

$$MoO_3 + 2Al = Mo + Al_2O_3,$$
 (1)

$$3Nb_2O_5 + 10Al = 6Nb + 5Al_2O_3,$$
 (2)

$$3\text{Ta}_2\text{O}_5 + 10\text{Al} = 6\text{Ta} + 5\text{Al}_2\text{O}_3,$$
 (3)

$$Cr_2O_3 + 2Al = 2Cr + Al_2O_3,$$
 (4)

$$3V_2O_5 + 10Al = 6V + 5Al_2O_3,$$
 (5)

$$3\text{TiO}_2 + 4\text{Al} = 3\text{Ti} + 2\text{Al}_2\text{O}_3.$$
 (6)

The experiments used powder charges designed to produce five alloy compositions (S1–S5), as shown in Table 2.

Table 1. Selected characteristics of the primary powder components

Таблица 1. Некоторые характеристики основных исходных порошковых компонентов

Component	Grade	GOST/Technical specification (TU)	Particle size	Chemical composition, wt. %	
MoO ₃	Analytical reagent (ChDA)	TU 6-09-01-269-85	_	99.9	
Nb ₂ O ₅	Extra pure (OSCh (8-2))	TU 6-09-4047-86	_	99.9	
Ta ₂ O ₅	_	TU 48-4-408-78	<70 μm	99.9	
Cr_2O_3	Pure (Ch)	TU 6-09-4272-84	<20 μm	99.0	
V_2O_5	_	TU 6-09-4093-75	_	_	
TiO ₂	_	TU 6-09-2166-77	_	99.8	
Zr–Mo	_	Custom-made	<3 mm	Zr – 40.0 Mo – balance	
Hf–Mo	_	Custom-made	<3 mm	Hf – 40.0 Mo – balance	
Al	Aluminum powder (PA-4)	GOST 60-58-73	<130 μm	98.8	

the target RHEA alloy.

ducts formed a two-layer ingot with a well-defined interface. The upper part of the ingot (slag layer) consisted of fused corundum, while the lower part was

The application of overload during the combustion stage of thermite-type SHS mixtures made it possible to significantly reduce, or even completely suppress, the dispersion of combustion products. It also ensured intensive mixing of the high-temperature melt behind the combustion front, enabling high conversion of the starting mixture directly within the combustion zone. The action of overload during the gravitational separation and subsequent cooling stages led to a high yield of the metallic phase in the ingot – approaching the theoretical value - and facilitated the removal of gaseous reaction products. In addition, overload promotes homogeneous distribution of the chemical elements throughout the volume of the resulting ingot, which is critically important for the synthesis of multimetallic alloys. The combustion process was recorded using a video camera mounted on the rotor of the centrifugal SHS setup.

Phase composition was analyzed using an ARL X'TRA X-ray diffractometer. Elemental distribution within the structural constituents of the synthesized RHEAs, as well as energy-dispersive spectroscopy (EDS) analysis, were performed using a Zeiss Ultra Plus ultra-high-resolution field emission scanning electron microscope (based on the Ultra 55 platform), equipped with an EDS detector capable of generating elemental mapping across the sample surface.

2. Results and discussion

2.1. Thermodynamic analysis

An important parameter in the development of SHS system formulations is the thermodynamic assessment of the maximum achievable synthesis temperature (adiabatic temperature) at various ratios of starting components. This evaluation helps determine the range of component ratios that meet the necessary conditions for obtaining cast final synthesis products. One such condition is that the adiabatic temperature of synthesis must exceed the melting points of the final and intermediate reaction products. It is important to note that the calculated combustion temperature is always somewhat higher than the actual experimental synthesis temperature. This discrepancy arises from heat losses due to thermal exchange with the mold material, incomplete chemical reactions (i.e., partial conversion of the reactants), shifts in component concentrations caused by partial gas evolution (primarily suboxides), and possible ejection of reaction products during

When Zr-Mo and Hf-Mo master alloys were introduced into the charge, the composition was adjusted based on the total molybdenum content. Aluminum served as the reducing agent, while CaO and CaF, were used as fluxing additives. The required amount of flux to bind Al₂O₃ and form a low-melting-point slag system during melting was calculated from the total amount of aluminum oxide generated in reactions (1)-(6). The mass of the starting mixture was constant across all experiments and amounted to 600 g. The concentration of the added flux varied from 2 to 5 wt. %. To synthesize the alloys in combustion mode, hollow cylindrical refractory molds made of sintered electrolytic corundum (Al₂O₃) were used. These molds had an inner diameter of 80 mm and a height of 170 mm and were pre-dried for at least 1 h at 90 °C. During the filling process, the powder charge (500 g) was compacted by vibration into the mold. The loaded mold was then placed on the rotor of a centrifugal SHS setup. Combustion synthesis of the prepared mixtures was carried out in a custom-designed centrifugal SHS unit [43; 45], specifically developed for producing cast materials via centrifugal SHS metallurgy. It was previously shown [43] that the optimal range of centrifugal acceleration (hereinafter referred to as overload) for synthesizing alloys based on refractory metals is between 55 and 65g.

To generate the required centrifugal acceleration, the rotor was driven by an electric motor to a preset rotational speed, producing a g-force within the specified range. The reaction mixture was then ignited using a short laser pulse focused on the sample surface. Combustion proceeded at a constant rotor speed in an open-type reaction mold under atmospheric pressure. The combustion temperature exceeded 3000 K, which was higher than the melting points of the final products. After the reaction, the molten products (the alloy and the alumina-based slag) separated due to their mutual immiscibility and the action of centrifugal forces and then solidified upon cooling. Cooling of the reaction mass was forced through a water-cooled jacket of the reaction chamber. The combustion pro-

Table 2. Calculated chemical composition, wt. % Таблица 2. Расчетный химический состав, мас. %

Composition	Mo	Nb	Та	Cr	V	Zr	Hf
S1	34.35	33.26	32.39	_	_	_	_
S2	31.46	30.47	28.77	9.30	_	_	_
S3	28.29	27.39	25.69	13.06	5.57	_	_
S4	23.30	22.57	35.16	10.10	_	8.87	_
S5	21.82	22.82	32.92	9.46	_	_	12.98



the high-temperature interaction of the initial components in the combustion front.

To theoretically assess the maximum achievable synthesis temperature (adiabatic temperature) as a function of the initial component ratios, a thermodynamic analysis of the synthesis processes was performed using the THERMO software package developed at ISMAN. This software allows thermodynamic equilibrium calculations in complex multicomponent heterophase systems. It includes a database of thermodynamic data for equilibrium calculations and features a function for adding data for new compounds [46; 47]. The calculation results include the equilibrium composition of reaction products (both condensed and gaseous) and the adiabatic temperature. The software enables thermodynamic calculations under isobaric, isochoric, or isothermal conditions, depending on the selected mode. The studied systems can be either gas-free or contain any amount of gaseous phase.

The results of the thermodynamic analysis of the adiabatic temperature $(T_{\rm ad})$ and the total concentrations of the gas (gas), metallic (ingot), and oxide (oxide) phases in the reaction products for the investigated systems S1–S5 (see Table 2) are presented in Fig. 1.

Analysis of the obtained data revealed that for systems S1–S3, the combustion temperature of the mixtures can reach or exceed 3000 K (3427–2935 K), which is higher than the melting points of all alloy components ($T_{\rm melt}$, K: Nb – 2741, Mo – 2896, Cr – 2163, Zr – 2125, V – 2170, Hf – 2506), with the exception of tantalum (Ta – 3290 K). However, the presence of a high-temperature liquid phase formed by these

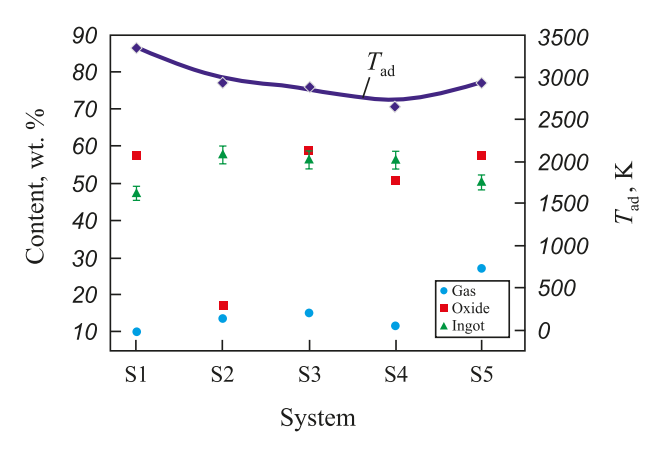


Fig. 1. Thermodynamic analysis of the adiabatic temperature ($T_{\rm ad}$) and the relative amounts of gaseous, metallic, and oxide phases in the combustion products for systems S1–S5

Рис. 1. Термодинамический анализ адиабатической температуры $(T_{\rm ag})$ и соотношения в продуктах горения газовой, металлической и оксидной фаз для систем S1–S5

components is likely to promote rapid dissolution of finely dispersed solid-phase tantalum particles that form in the combustion front. In the case of system S5, the adiabatic combustion temperature is somewhat lower ($T_{\rm ad} = 2890.8~{\rm K}$), which may result in Ta and Nb remaining partially in the solid state. Nonetheless, as in the previous systems, the presence of molten phases from other alloy components should enable their rapid and complete dissolution in the resulting alloy ingot. This assumption will be tested in the experimental section of this study.

Across all the studied systems, the mass fractions of oxide and metallic phases vary only slightly (see Fig. 1), which is a favorable factor for their comparative evaluation in the experimental work.

The analysis of the calculated adiabatic temperatures and component concentrations under thermodynamic equilibrium conditions showed that the combustion temperature can reach up to 3427 K for systems S1–S3 (see Table 2), and up to 2935 K for system S5. Thus, it can be concluded that there are no thermodynamic limitations to producing cast materials in the studied systems (S1–S5); the combustion temperatures are sufficient to obtain materials with the desired (target) composition.

2.2. Effect of centrifugal acceleration (overload) on the composition and microstructure formation of RHEAs

As shown in previous studies [40–44], the level of overload can have a significant impact on the macroscopic kinetics of the synthesis process and, consequently, on the resulting composition and microstructure of cast alloys. In the case of alloys based on refractory metals, the lifetime of the high-temperature melt in its liquid state is relatively short, as these systems have considerably higher crystallization temperatures compared to transition-metal-based alloys. Therefore, to ensure proper formation of the ingot in the bottom part of the mold, it is essential to accelerate the phase separation between the metallic (ingot) and oxide (Al₂O₂-based corundum) phases. The most effective way to achieve this is by applying centrifugal forces generated by centrifugal SHS units during both the combustion stage and the phase separation of synthesis products.

Fig. 2 presents data for the base system S1 (Mo, Nb, Ta), showing how the combustion rate (U_c), the metallic phase yield in the ingot (η_1), and the loss of combustion products due to dispersion (η_2) depend on the applied centrifugal acceleration g. The results clearly demon-

Sanin V.N., Ikornikov D.M., and etc. Synthesis of refractory high-entropy alloys based ...

strate that the combustion rate of the base composition increases significantly under overload, particularly in the range of 1 to 50g. Notably, the metallic phase yield also increases within this range, approaching a saturation level at values exceeding 100g. These findings indicate that applying overloads in the range of 50 to 100g is optimal for synthesizing the studied alloys.

Visual examination of the resulting samples confirmed that all of them exhibited a cast structure. Applying an overload greater than 50g ensured the formation of ingots with well-defined phase separation. At overloads below 50g, the ingots developed an irregular macrostructure, with gas inclusions observed in their upper sections. As a result, an overload of 60g was selected for synthesizing the target compositions S2–S5.

Video analysis of the combustion process for S2-S5 showed no significant increase (exceeding 15%) in the combustion rate.

2.3. Chemical and phase analysis of the synthesized RHEAs

The cast RHEA samples (S1–S5), after removal from the refractory mold, were sectioned transversely and subjected to analysis. Elemental composition analysis (Table 3), performed by *X*-ray fluorescence spectroscopy, confirmed the presence of the target elements Mo, Nb, Ta, Cr, V, Zr, and Hf in the synthesized alloys. The deviation of their concentrations from the calculated values did not exceed 1 wt. %. It should be noted that the use of Zr–Mo and Hf–Mo master

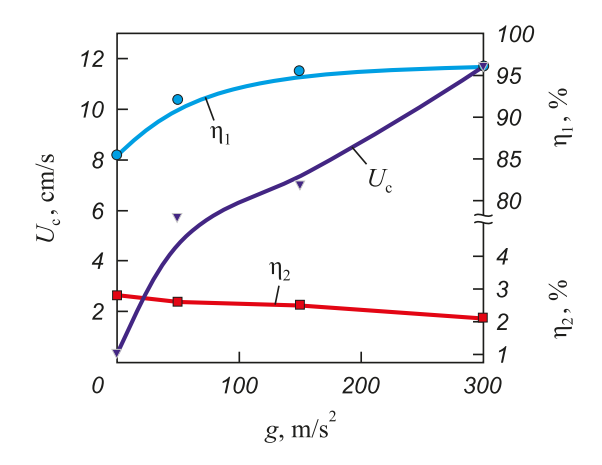


Fig. 2. Effect of overload (g) on the combustion rate (U_c) , the yield of the metallic phase in the ingot (η_1) , and the combustion product loss (η_2) for the base S1 system (see Table 2)

Рис. 2. Влияние величины перегрузки (g) на скорость горения (U_r) , полноту выхода металлической фазы в слиток (η_1) и величину потерь продуктов горения (η_2) для базовой системы S1 (см. табл. 2)

alloys helped minimize the interaction of chemically active components (Zr and Hf) within the combustion front, thus enabling their incorporation into the alloy at concentrations close to the theoretical values.

For comparative analysis, a binary Mo–Nb alloy designated as S0 was synthesized. The *X*-ray diffraction patterns of the RHEA samples (S0–S5) are shown in Fig. 3.

The results of X-ray diffraction (XRD) analysis for the S0–S5 alloys are summarized in Table 4. The phase composition of the metallic ingots depends on the specific combination of alloying elements. The co-reduction and subsequent alloying of group V metals (Nb, Ta, V) with group VI metals (Cr, Mo) result in the formation of nearly single-phase alloys with a body-centered cubic (BCC) crystal structure, which is typical for these elements. It is well established that one of the key conditions for the formation of a single-phase solid solution is that the constituent metals share the same crystal structure type.

The XRD pattern of the binary S0 (Mo + Nb) alloy (Fig. 3) confirms the formation of the MoNb phase (space group *Im-3m*, PDF2 card #65-5786). Indeed, the Mo–Nb binary system exhibits unlimited mutual solubility and conforms to the Hume–Rothery rules for the formation of substitutional solid solutions. A small amount of impurity phases, such as Al₂O₃ and NbO, was also detected, likely due to incomplete phase separation during ingot formation.

The addition of a third component (Ta) to alloy S1 also results in the formation of a BCC solid solution phase, MoNbTa. The diffraction peaks of this phase are shifted toward lower angles, indicating an increase in its unit cell parameter compared to the binary MoNb solid solution. This increase is attributed to the larger atomic radius of Ta (1.430 Å) relative to Mo (1.362 Å) and Nb (1.429 Å) [14]. Weak diffraction peaks of the Al₂Nb₃Mo₃ phase with a cubic structure (space

Table 3. Chemical composition of synthesized RHEAs ingots (wt. %)

Таблица 3. Химический состав синтезированных слитков ТВЭС (мас. %)

Alloy	Mo	Nb	Ta	Cr	V	Zr	Hf
S0	50.8	49.2	_	_	-	_	_
S1	34.7	33.4	31.9	_	_	_	_
S2	31.9	30.9	28.1	9.1	_	_	_
S3	28.6	27.9	25.1	12.7	5.7	_	_
S4	23.7	22.8	35.2	9.7	_	8.6	_
S5	22.5	23.6	32.2	9.3	_	_	12.4



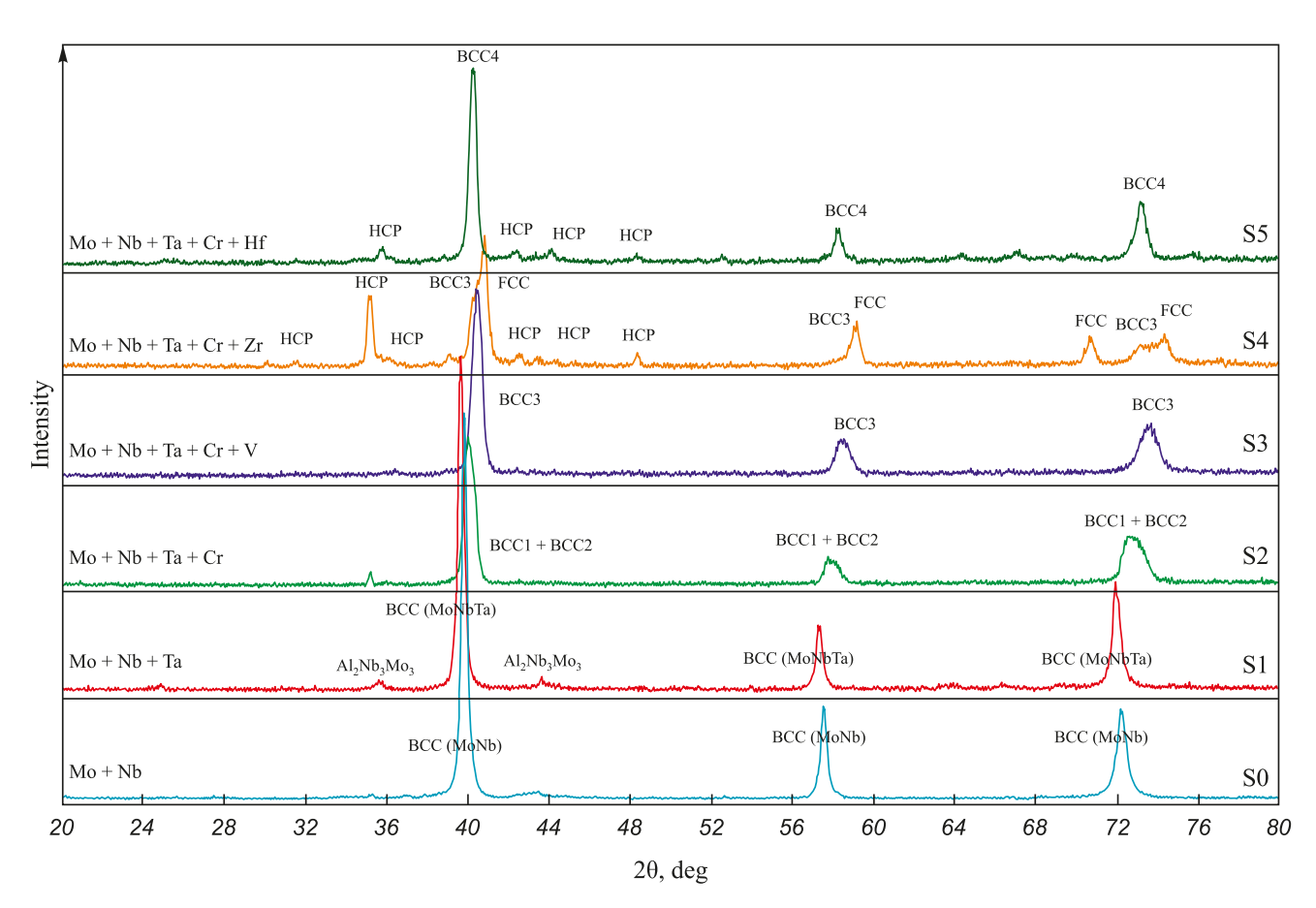


Fig 3. XRD patterns of the synthesized RHEA samples (S0–S5)

Рис. 3. Дифрактограммы синтезированных образцов ТВЭС (S0–S5)

Table 4. Phase composition of RHEAs ingots Таблица 4. Фазовый состав слитков ТВЭС

Alloy	Main phases	Secondary phases	Impurity phases
S0	MoNb	_	Al ₂ O ₃ , NbO
S1	MoNbTa (BCC solid solution)	Al ₂ Nb ₃ Mo ₃	_
S2	MoNbTaCr (BCC1 + BCC2 solid solution)	_	ТаО
S3	MoNbTaCrV (BCC3 solid solution)	_	NbO
S4	MoNbTaCrZr (FCC + BCC3 solid solution)	НСР	_
S5	MoNbTaCrHf (BCC4 solid solution)	НСР	_

group *Pm*-3*n*, PDF2 card #65-4465) are also observed in the XRD pattern of alloy S1 (Fig. 4).

The addition of a fourth component (Cr) to alloy S2 leads to the formation of two BCC solid solution phases with similar unit cell parameters, designated as BCC1 and BCC2 in Fig. 3. The corresponding diffraction peaks are significantly broadened due to the overlap of reflections from both phases. Notably, the peaks are shifted toward higher angles, indicating a reduction in the unit cell parameter. This can be attributed to the presence of Cr in the solid solution, as Cr has a substantially smaller atomic radius

(1.249 Å) than the other elements in the alloy. The difference in unit cell parameters between BCC1 and BCC2 suggests varying Cr content in the two phases, as confirmed by the microanalysis data shown in Fig. 5. Crystallization occurs from the melt, where a homogeneous distribution of Mo, Nb, Ta, and Cr is established. It is likely that the two-phase structure forms over a temperature range in which the Cr-depleted, refractory-rich phase (Mo–Nb–Ta) solidifies first, followed by a Cr-enriched, lower-melting phase. It is known that in multicomponent systems, the formation of a single-phase solid solution requires that the atomic radius



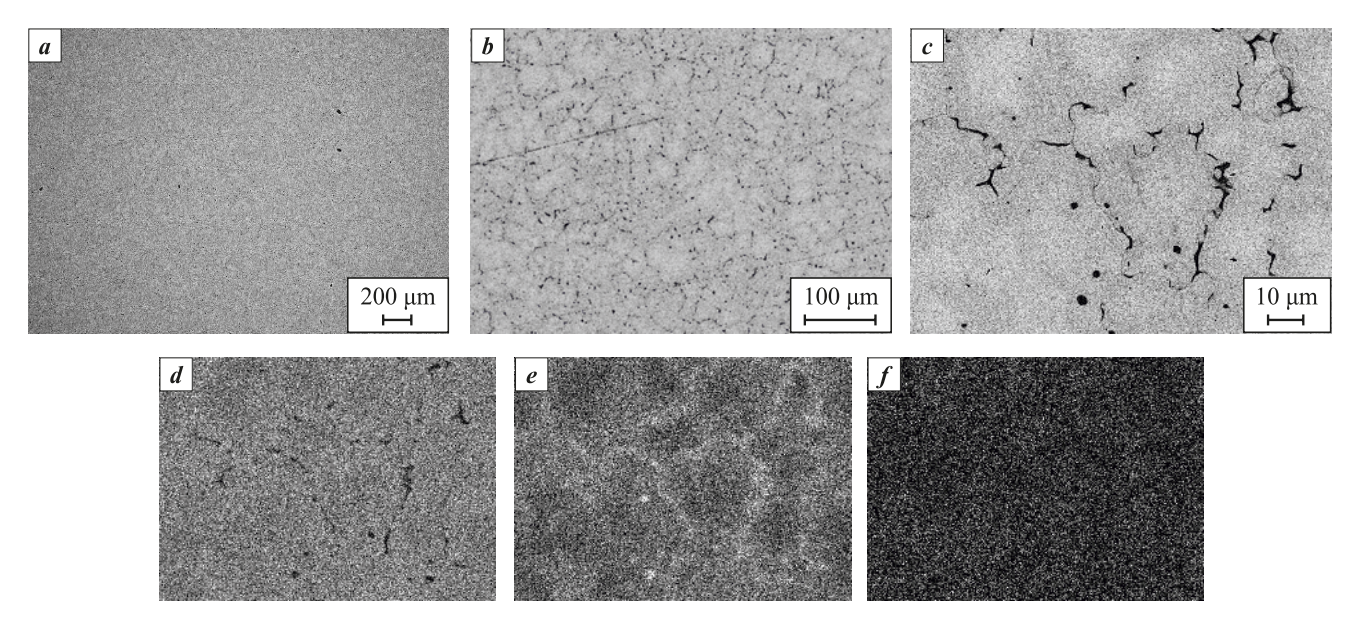


Fig. 4. Microstructure of alloy S1 (a, b) and elemental distribution maps of the obtained alloy (c-f) c – combined image of elemental distribution map, d – Mo, e – Nb, f – Ta

Рис. 4. Микроструктура сплава состава S1 (a, b) и карты распределения элементов полученного сплава (c-f) c – комбинированное изображение карты распределения элементов, d – Mo, e – Nb, f – Ta

difference between constituent elements not exceed 4 %. This condition is not met with Cr addition, which explains the formation of a two-phase alloy.

Introducing a fifth component (V) into alloy S3 results in the formation of a group of BCC phases, collectively referred to as BCC3 in the XRD pattern. The observed reflections are symmetric but significantly

broadened, indicating the presence of multiple BCC phases with different elemental compositions and corresponding unit cell parameters. Although the atomic radius of V (1.316 Å) is larger than that of Cr, the criteria for single-phase formation are still not satisfied. The peak shift toward higher angles is the most pronounced in this alloy, suggesting that the average unit

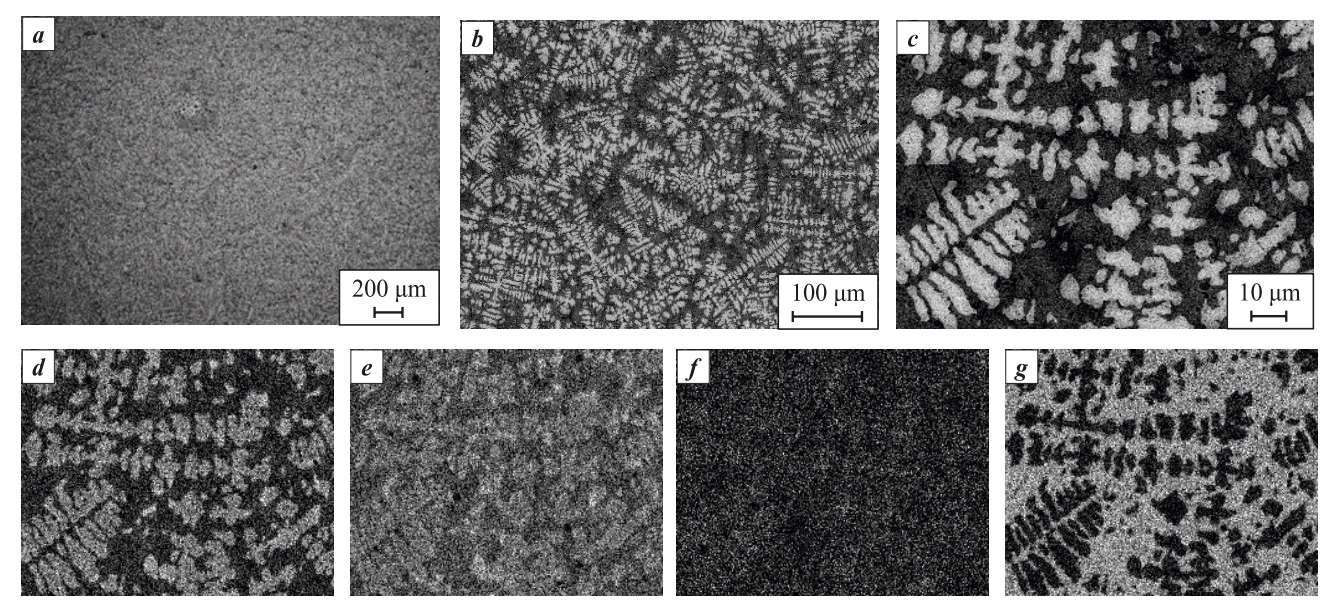


Fig. 5. Microstructure of alloy S2 (a, b) and elemental distribution maps of the obtained alloy (c-g) c – combined image of elemental distribution map, d – Mo, e – Nb, f – Ta, g – Cr

Рис. 5. Микроструктура сплава состава S2 (a, b) и карты распределения элементов полученного сплава (c-g) c – комбинированное изображение карты распределения элементов, d – Mo, e – Nb, f – Ta, g – Cr



cell parameter of the BCC phases in the five-component system is the lowest among the MoNb, MoNbTa, and MoNbTaCr alloys.

The addition of group IV elements (Zr and Hf), which have a hexagonal crystal structure, to the fourcomponent alloy S2 (MoNbTaCr) causes significant changes in the phase composition of alloys S4 and S5, respectively. In the Zr-containing five-component alloy S4, the XRD pattern shows, in addition to BCC reflections, strong peaks of an FCC phase (space group Fm-3m) and weak peaks of two hexagonal (HCP) phases (space groups P-6m2 and $P6_2/mmc$). The PDF2 Realize 2022 diffraction database does not list compounds containing these elements in the observed combinations with these specific space groups. For the Hf-containing alloy S5, intense reflections of a BCC4 phase are observed, with angular positions close to those of the BCC3 phase, indicating similar unit cell parameters. As in the Zr-containing alloy, weak reflections of two HCP phases are also present. Clearly, the formation of multiphase structures in alloys S4 and S5 is a result of the differing crystal structures of the alloying elements – BCC for group V and VI metals (Mo, Nb, Ta, Cr) and HCP for group IV metals (Zr and Hf). Moreover, the atomic radii of Zr (1.603 Å) and Hf (1.578 Å) are significantly larger than those of the BCC-forming elements.

2.4. Microstructure of the synthesized RHEAs (S1–S5)

Microstructural analysis was performed on prepolished cross-sections of the cast RHEA samples (S1–S5). Elemental distribution maps were obtained using energy-dispersive *X*-ray spectroscopy (EDS). The results are shown in Figs. 4–8.

Microstructural analysis of the cast RHEA samples (S1–S5) revealed that the addition of modifying elements (Cr, V, Zr, and Hf) leads to the formation of new structural features.

The base alloy S1 (Fig. 4, *a*, *b*) exhibits a fairly uniform elemental distribution, indicating a single-phase microstructure, which is consistent with the XRD results. Elemental mapping (Fig. 4, *c*–*f*) shows only slight Nb enrichment at the grain boundaries, a common characteristic of cast materials.

The introduction of Cr into the base composition (Fig. 5) causes noticeable structural changes in alloy S2. The micrographs reveal a two-phase microstructure, which agrees with the XRD data. This structure comprises two BCC solid solutions (see Fig. 3): one forms a Cr-rich matrix, and the other is a Mo-based dendritic phase.

With the addition of both Cr and V to the base alloy (Fig. 6), alloy S3 exhibits a similar dendritic structure. However, the dendrite arm size is slightly reduced, ranging from 5 to 10 μ m.

The combined addition of Cr and Zr to the base composition leads to significant changes in the phase composition of alloy S4. According to the XRD data (Fig. 3), three distinct phases form: two BCC solid solutions and one FCC solid solution. However, microstructural examination (Fig. 7) shows two clearly distinguishable components: the first (Fig. 7, c–h, bright regions) exhibits an equiaxed grain structure and is based on a Mo–Ta solid solution, while the second forms an intergranular network enriched in Cr and Zr.

In the case of alloy S5, where both Cr and Hf are introduced, XRD analysis (Fig. 3) indicates the formation of a single-phase BCC solid solution. Microstructural observations (Fig. 8) confirm a relatively homogeneous distribution of the primary elements. Nevertheless, elemental mapping (Fig. 8, c–h) reveals localized Hf-rich precipitates with sizes of 3–5 μ m. Chromium is present as dispersed intragranular particles and thin bands along grain boundaries.

The fine-dispersed microstructure observed in alloys S2–S5 is expected to contribute to enhanced mechanical properties.

The objective of this study did not include measuring the physicochemical or mechanical properties of the alloys, as the primary goal was to confirm the feasibility of synthesizing such RHEAs based on three refractory components (Mo–Nb–Ta) by centrifugal SHS metallurgy using oxide feedstock. This feasibility was successfully demonstrated, and the next stage of research will focus on establishing structure–property relationships.

2.5. Oxidation resistance of the synthesized alloys S2–S5

The oxidation resistance of the synthesized refractory high-entropy alloys (RHEAs) S1–S5 (see Table 2) was investigated under cyclic heating and holding at 1000 °C in an air atmosphere. It is worth noting that most studies on RHEA oxidation behavior are conducted under isothermal conditions. While such conditions are suitable for evaluating oxidation kinetics and mechanisms, they do not adequately simulate the repeated heating—cooling cycles that these materials typically experience in real-world service environments.

Disk-shaped samples with a diameter of 8 mm and a height of 4 mm were cut from the cast ingots using a GX-320L electrical discharge machine (CHMER



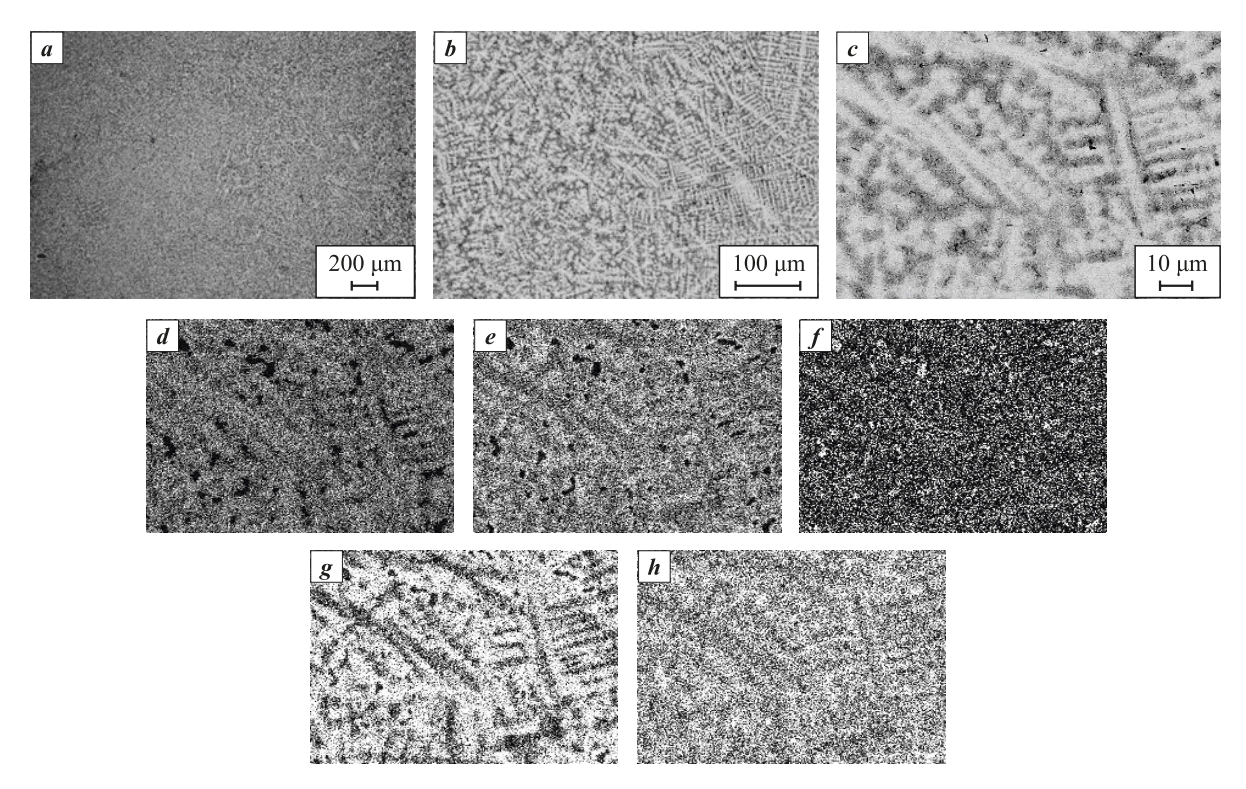


Fig. 6. Microstructure of alloy S3 (a, b) and elemental distribution maps of the obtained alloy (c-h) c – combined image of elemental distribution map, d – Mo, e – Nb, f – Ta, g – Cr, h – V

Рис. 6. Микроструктура сплава состава S3 (a, b) и карты распределения элементов полученного сплава (c-h) c – комбинированное изображение карты распределения элементов, d – Mo, e – Nb, f – Ta, g – Cr, h – V

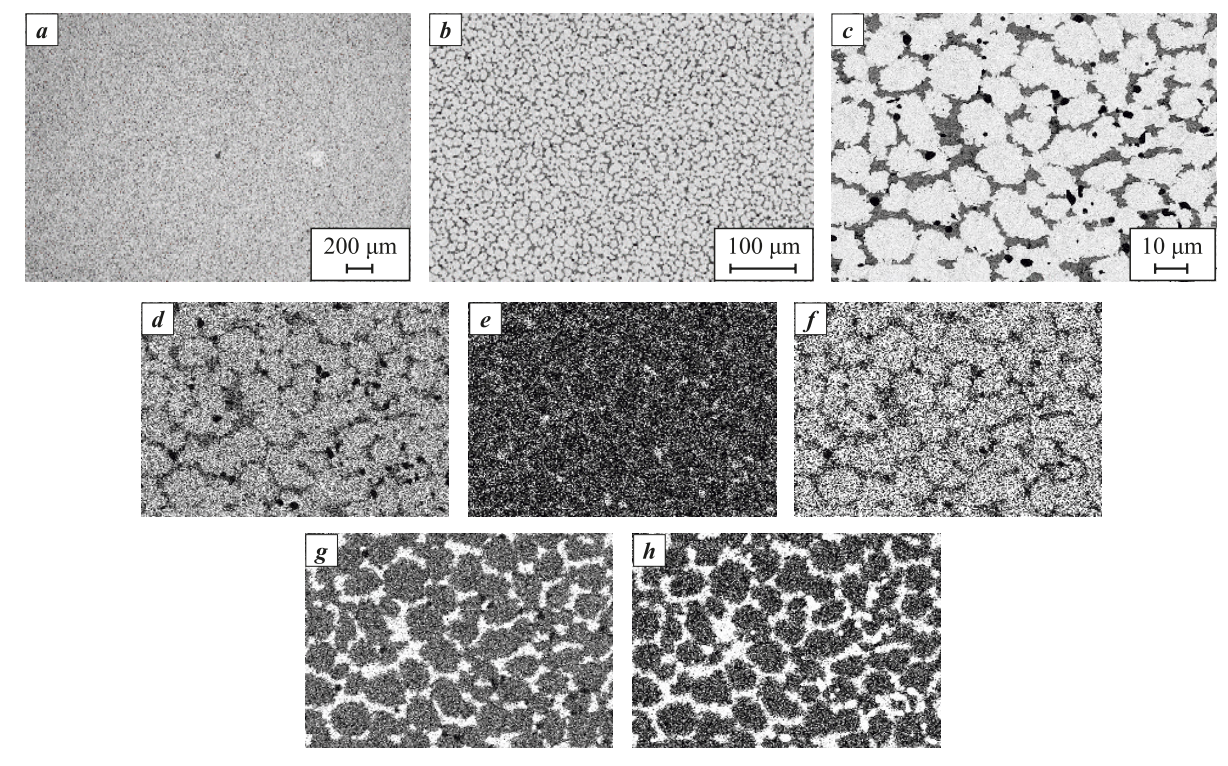


Fig. 7. Microstructure of alloy S4 (a, b) and elemental distribution maps of the obtained alloy (c-h) c – combined image of elemental distribution map, d – Mo, e – Nb, f – Ta, g – Cr, h – Zr

Рис. 7. Микроструктура сплава состава S4 (a, b) и карты распределения элементов полученного сплава (c-h) c – комбинированное изображение карты распределения элементов, d – Mo, e – Nb, f – Ta, g – Cr, h – Zr



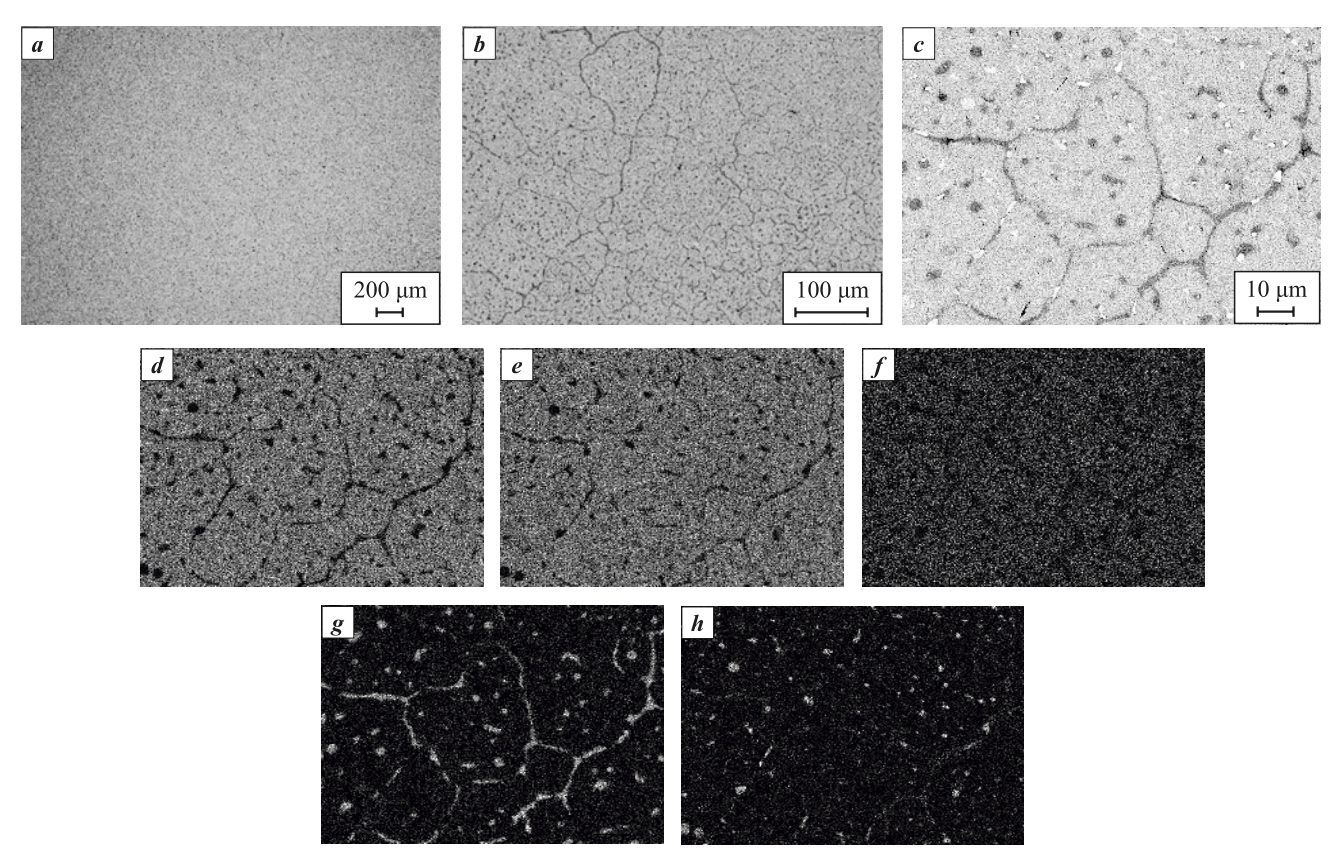


Fig. 8. Microstructure of alloy S5 (a, b) and elemental distribution maps of the obtained alloy (c-h) c – combined image of elemental distribution map, d – Mo, e – Nb, f – Ta, g – Cr, h – Hf

Рис. 8. Микроструктура сплава состава S5 (a, b) и карты распределения элементов полученного сплава (c-h) c – комбинированное изображение карты распределения элементов, d – Mo, e – Nb, f – Ta, g – Cr, h – Hf

EDM, China). The samples were then ground to a surface roughness of $R_z = 5$, followed by ultrasonic cleaning in isopropanol.

The oxidation annealing tests were carried out in a programmable muffle furnace. The samples were placed on alumina ceramic supports and arranged in a "cassette" fixture to enable convenient and rapid insertion/removal from the furnace. The cassette was loaded into a preheated furnace and held according to the following schedule: 30 min per cycle during the first hour, followed by 1 h cycles until a total annealing time of 10 h was reached. After each oxidation cycle, the samples were air-cooled to room temperature and weighed using an analytical balance with a precision of 0.1 mg. The mass gain per unit surface area over time was determined. Oxidation kinetics curves were constructed based on the experimental data. The appearance of the samples after 10 h of oxidation is shown in Fig. 9.

Visual examination revealed that the S1, S4, and S5 alloys underwent complete structural degradation. In contrast, the S2 alloy showed only partial loss of structural integrity, while the S3 alloy retained its

original shape and developed only a dense oxide layer on its surface.

Since alloy S3 exhibited the lowest degree of oxidation, a cross-section of its sample was prepared to investigate the structure of the oxidized and transitional zones. The remaining samples were pulverized, and their powders were subjected to XRD analysis (Table 5). The results indicate that in the oxidized alloys S4 and S5, the primary oxidation product is the rutile-type phase CrTaO₄, which forms via a reaction between Cr2O3 and Ta2O5. According to the literature [48], unlike conventional oxides such as Al₂O₃ and Cr₂O₃ – which typically form dense, continuous surface layers during high-temperature oxidation of heat-resistant alloys - CrTaO₄ tends to form as discontinuous flakes. Although it does not prevent internal oxidation, it effectively hinders the outward diffusion of metallic cations. In contrast, another rutile-type oxide, CrNbO₄, is known to enhance oxidation resistance [49], which is consistent with our experimental observations: in alloy S2 (Mo-Nb-Ta-Cr), CrNbO₄ was identified as the predominant oxidation phase. As shown in Fig. 9, the S2 sample partially retained its shape, in contrast to the S1, S4, and S5 alloys.



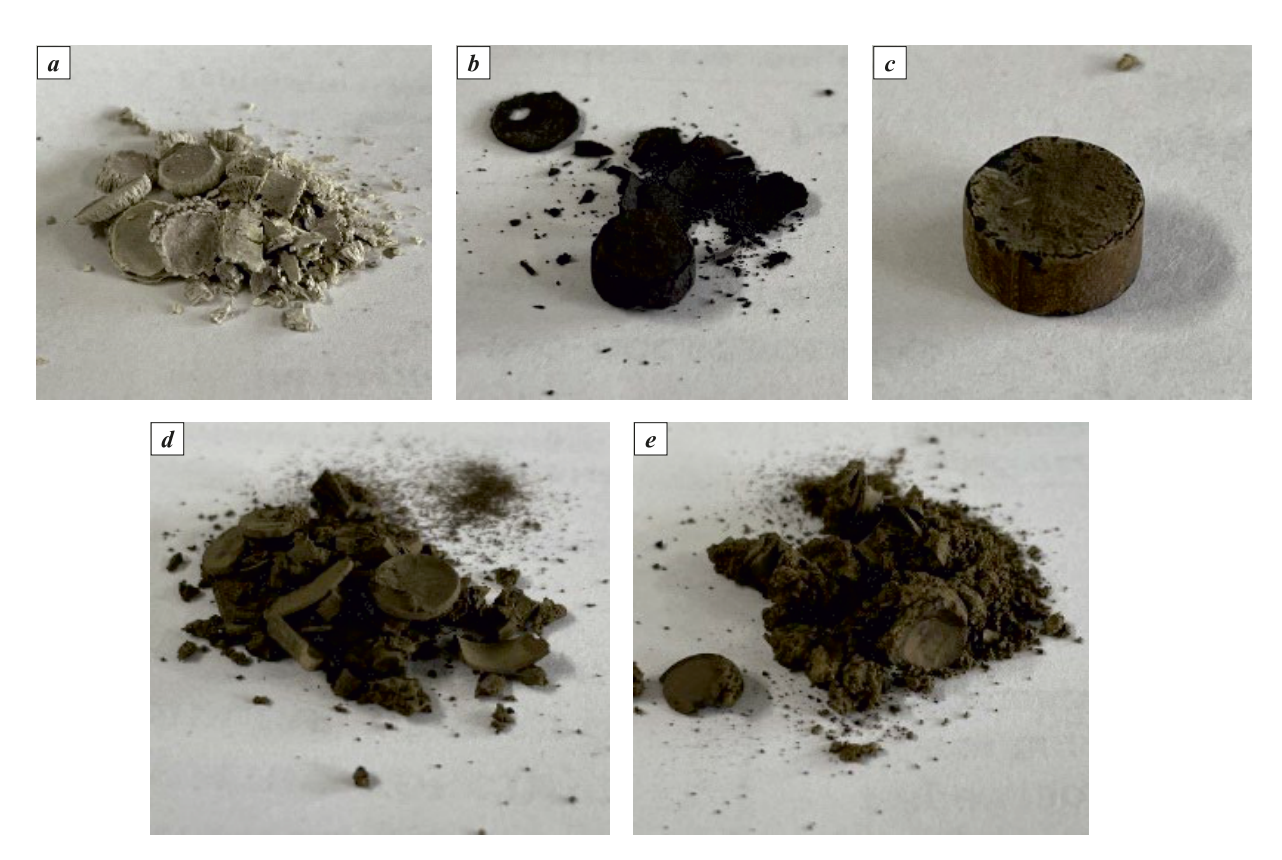


Fig. 9. Appearance of the tested RHEA samples after oxidation annealing (T = 1273 K, $\tau = 10 \text{ h}$) a - S1 (Mo-Nb-Ta); b - S2 (Mo-Nb-Ta-Cr); c - S3 (Mo-Nb-Ta-Cr-V); d - S4 (Mo-Nb-Ta-Cr-Zr); e - S5 (Mo-Nb-Ta-Cr-Hf)

Рис. 9. Внешний вид испытуемых образцов ТВЭС после проведения окислительного отжига (T = 1273 K, $\tau = 10 \text{ ч}$) a - S1 (Mo-Nb-Ta); b - S2 (Mo-Nb-Ta-Cr); c - S3 (Mo-Nb-Ta-Cr-V); d - S4 (Mo-Nb-Ta-Cr-Zr); e - S5 (Mo-Nb-Ta-Cr-Hf)

The mass change data for the tested samples are shown in Figs. 10 and 11. Analysis of these data revealed anomalous behavior in the single-phase base alloy S1 (Mo–Nb–Ta). This sample exhibited a significant mass loss during annealing (Fig. 10), especially within the first 5 h.

It is well established that Mo-based alloys are susceptible to oxidation at temperatures above 773 K due to the formation of volatile MoO₃. The Mo content in alloy S1 is the highest among all samples (34.35 wt. %), and notably, it lacks chromium, which can form protective complex oxides. As a result, the intense oxidation

Table 5. Phase composition of oxidation products after annealing ($T=1273~{\rm K},\, \tau=10~{\rm h}$) *Таблица 5.* Фазовый состав окисленных продуктов после отжига ($T=1273~{\rm K},\, \tau=10~{\rm y}$)

Alloy	Composition	Main phase Secondary phases		Oxidation
S1	Mo–Nb–Ta	MoTa ₁₂ O ₃₃ (PDF2 card #000-89-6894)	_	Complete
S2	Mo-Nb-Ta-Cr	CrNbO ₄ (PDF2 card #000-81-0909)	Mo ₁₃ O ₃₃ (PDF2 card #000-82-1930), MoNb (BCC, space group <i>Im-3m</i> , PDF2 card #000-65-5786)	Partial
S4	Mo-Nb-Ta-Cr-Zr	CrTaO ₄ (PDF2 card #000-39-1428)	TaZr _{2,75} O ₈ (PDF2 card #000-42-0060), Mo ₁₃ O ₃₃ (PDF2 card #000-82-1930)	Complete
S5	Mo-Nb-Ta-Cr-Hf	$\begin{array}{c} \text{CrTaO}_4 \\ \text{PDF2 card } \#000\text{-}39\text{-}1428) \end{array} \\ \begin{array}{c} \text{Nb}_4 \text{Ta}_2 \text{O}_{15} \\ \text{(PDF2 card } \#000\text{-}15\text{-}0114), \\ \text{HfO}_2 \\ \text{(PDF2 card } \#000\text{-}53\text{-}0560) \end{array}$		Complete



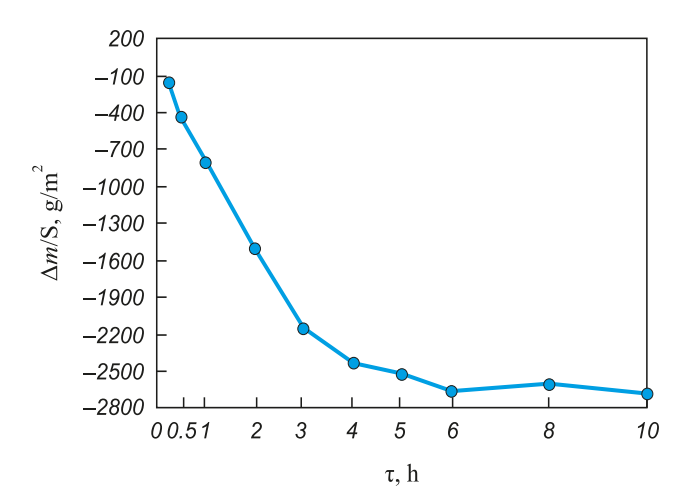


Fig. 10. Mass change of the S1 alloy (Mo–Nb–Ta) sample during oxidation annealing (T = 1273 K, $\tau = 10 \text{ h}$)

Рис. 10. Изменение массы испытуемого образца сплава S1 (Мо–Nb–Ta) при окислительном отжиге (T = 1273 K, τ = 10 ч)

of molybdenum leads to considerable mass loss due to the volatilization of Mo. This assumption is supported by the XRD data.

Analysis of the data presented in Fig. 11 shows that the oxidation behavior of the alloys varies both qualitatively (mass gain or loss) and quantitatively depending on their composition. Alloys S4 and S5 exhibited the greatest mass gain during the first 5 h of exposure; thereafter, a non-monotonic oxidation trend was observed, and at $\tau > 5$ h, they began to lose mass. Among all tested samples, alloy S3 showed the smallest mass change, which made the investigation of its structure near the oxidation zone particularly relevant.

Microstructural analysis based on cross-sectional micrographs (Fig. 12) reveals that the interface between the oxidized layer and the bulk alloy is well defined. A distinct transition zone is practically absent. Elemental distribution data (Fig. 12, *c*–*h*) indicate that the most significant compositional change in the oxidized layer is observed for Mo, whose concentration is minimized due to the volatility of the molybdenum oxide. The other elements (Nb, Ta, Cr, and V), according to the XRD data, retain their concentrations while transitioning to oxidized states and forming complex oxides.

These findings suggest that the S3 alloy (Mo–Nb–Ta–Cr–V) is the most promising candidate for further research. Compared to other compositions reported in the literature, it demonstrates superior oxidation resistance [50]. With further optimization of the alloying system, its oxidation resistance could be improved even more, making this material a strong contender for high-temperature applications. As previously noted, oxidation resistance is just one of the key

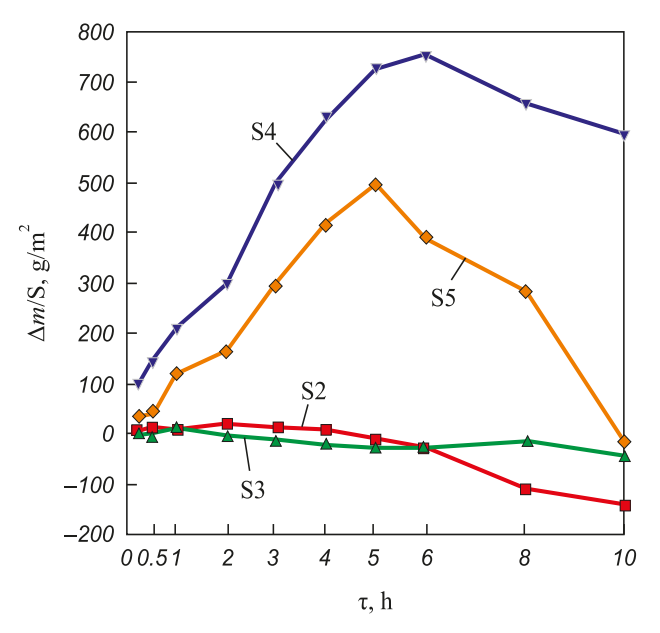


Fig. 11. Mass change curves for the S2–S5 alloy samples during oxidation annealing (T = 1273 K, τ = 10 h)
 Compositions: Mo–Nb–Ta–Cr (S2); Mo–Nb–Ta–Cr–V (S3); Mo–Nb–Ta–Cr–Zr (S4); Mo–Nb–Ta–Cr–Hf (S5)

Рис. 11. Кривые изменения массы испытуемых образцов S2–S5 при окислительном отжиге ($T=1273~{\rm K},\, \tau=10~{\rm y}$) Составы: Mo–Nb–Ta–Cr (S2); Mo–Nb–Ta–Cr–V (S3); Mo–Nb–Ta–Cr–Zr (S4); Mo–Nb–Ta–Cr–Hf (S5)

performance parameters for refractory high-entropy alloys (RHEAs), and future studies will aim to evaluate other relevant properties.

Conclusion

This study experimentally demonstrated the feasibility of producing cast refractory high-entropy alloys (RHEAs) by self-propagating high-temperature synthesis (SHS) metallurgy – one of the technological approaches within the SHS field. Using this method, cast RHEAs based on the Mo–Nb–Ta system, alloyed with 3d-transition metals (Cr, V, Zr, Hf), were obtained for the first time directly *in situ* via SHS. Microstructural analysis confirmed that all target elements were successfully incorporated and homogeneously distributed throughout the ingot volume. The overall elemental concentrations showed only minor deviations from the calculated chemical composition, indicating that the synthesis parameters were appropriately selected.

The introduction of modifying elements (Cr, V, Zr, and Hf) was found to induce the formation of new structural features, offering broad opportunities for tailoring the microstructure at the synthesis stage.

The experimental data confirm the potential of the investigated cast refractory high-entropy alloys (RHEAs) based on the Mo-Nb-Ta system and sup-



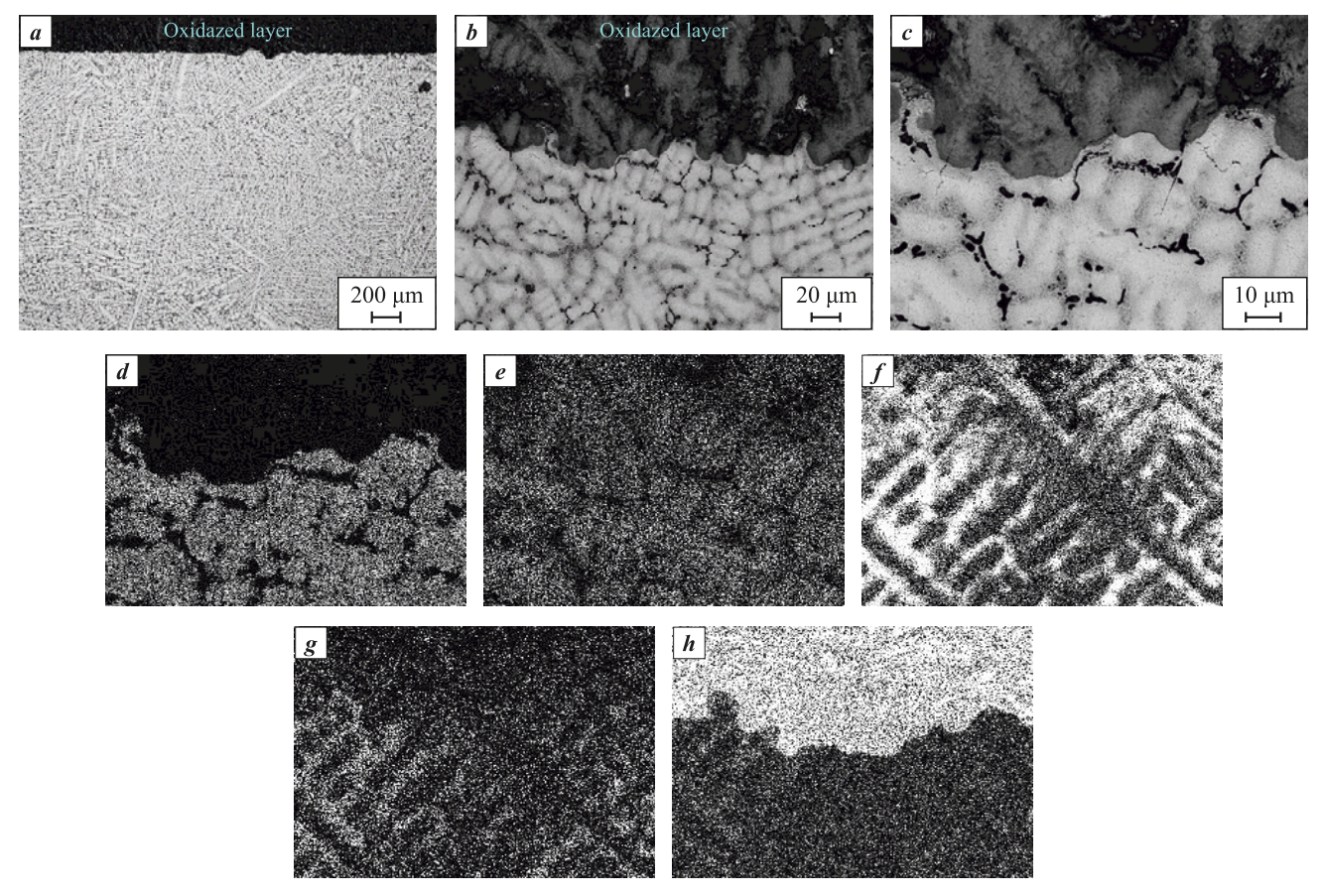


Fig. 12. Microstructure (a, b) of the surface layer of alloy S3 (Mo–Nb–Ta–Cr–V) after annealing $(T = 1273 \text{ K}, \tau = 10 \text{ h})$ and elemental distribution maps (c-h) c – combined image of elemental distribution map, d – Mo, e – Ta, f – Cr, g – V, h – O,

Рис. 12. Микроструктура (a, b) поверхностного слоя сплава S3 (Mo–Nb–Ta–Cr–V) после отжига (T = 1273 K, τ = 10 ч) и карты распределения элементов (c–h) c – комбинированное изображение карты распределения элементов, d – Mo, e – Ta, f – Cr, g – V, h – O $_2$

port the feasibility of the proposed alloy formation method via combustion synthesis using thermite-type SHS mixtures. This approach may serve as an effective alternative to energy-intensive vacuum electrometal-lurgical techniques. In light of increasingly stringent environmental regulations for metallurgical production – including the need for improved energy efficiency and reduced carbon footprint – the SHS-based centrifugal metallurgy method explored in this study fully aligns with these objectives.

It enables the production of cast RHEAs with high chemical homogeneity. The proposed method significantly simplifies the complex technological challenge of producing multicomponent cast RHEAs with controlled composition and targeted microstructural distribution. This can contribute to expanding the scientific basis for designing novel high-temperature metallic materials based on HEAs and for developing next-generation high-performance engineering systems.

Oxidation resistance testing revealed that alloy S3 (Mo–Nb–Ta–Cr–V) shows the greatest potential for further investigation. Compared to compositions reported by other researchers, it exhibited superior oxidation resistance, making it a promising candidate for high-temperature applications.

References / Список литературы

- 1. Cantor B., Chang I.T.H., Knight P., Vincent A.J.B. Microstructural development in equiatomic multicomponent alloys. *Journal of Materials Science and Engineering: A*. 2004;375–377:213–218.
 - http://doi.org/10.1016/j.msea.2003.10.257
- 2. Yeh J.W., Chen S.K., Lin S.J., Gan J.Y., Chin T.S., Shun T.T., Tsau C.H., Chang S.Y. Nanostructured highentropy alloys with multiple principal elements: Novel alloy design concepts and outcomes. *Advanced Engineering Materials*. 2004;6(5):299–303.

https://doi.org/10.1002/adem.200300567



- **3.** Yeh J.-W., Lin S.-J., Chin T.-S., Gan J.-Y., Chen S.-K., Shun T.-T., Tsau C.-H., Chou S.-Y. Formation of simple crystal structures in Cu–Co–Ni–Cr–Al–Fe–Ti–V alloys with multiprincipal metallic elements. *Metallurgical and Materials Transactions: A.* 2004;35A:2533–2536. https://doi.org/10.1007/s11661-006-0234-4
- **4.** Otto F., Yang Y., Bei H., George E.P.P. Relative effects of enthalpy and entropy on the phase stability of equiatomic high-entropy alloys. *Acta Materialia*. 2013;61(7):2628–2638. https://doi.org/10.1016/j.actamat.2013.01.042
- Zhang Y., Zuo T.T., Tang Z., Gao M.C., Dahmen K.A., Liaw P.K., Lu Z.P. Microstructures and properties of highentropy alloys. *Progress in Materials Science*. 2014; 61:1–93. https://doi.org/10.1016/j.pmatsci.2013.10.001
- Lu Y., Dong Y., Guo S., Jiang L., Kang H., Wang T., Wen B., Wang Z., Jie J., Cao Z., Ruan H., Li T. A promising new class of high-temperature alloys: Eutectic highentropy alloys. *Scientific Reports*. 2014;4:6200. https://doi.org/10.1038/srep06200
- 7. Murty B.S., Yeh J.W., Ranganathan S., Bhattacharjee P.P. High-entropy alloys. London: Elsevier, 2014. 213 p.
- **8.** Gorban F.F., Krapivka N.A., Firstov S.A. High-entropy alloys: Interrelations between electron concentration, phase composition, lattice parameter, and properties. *The Physics of Metals and Metallography*. 2017;118:970–981. https://doi.org/10.1134/S0031918X17080051
 - Горбань Ф.Ф., Крапивка Н.А., Фирстов С.А. Высокоэнтропийные сплавы электронная концентрация фазовый состав параметр решетки свойства. *Физика металлов и металловедение*. 2017;118(10):1017–1029.
- **9.** Brechtl J., Liaw P.K. (Eds.). High-entropy materials: Theory, experiments, and applications. Springer, 2021. https://doi.org/10.1007/978-3-030-77641-1
- 10. Gorban V.F., Krapivka N.A., Firstov S., Kurilenko D.V Role of various parameters in the formation of the physicomechanical properties of high-entropy alloys with bcc lattices. *Physics of Metals and Metallography*. 2018;119(5):477–481.
 - Горбань В.Ф., Крапивка Н.А., Фирстов С.А., Куриленко Д.В. Роль различных параметров в формировании физико-механических свойств высокоэнтропийных сплавов с ОЦК-решеткой. Физика металлов и металловедение. 2018;119(5):504–509.
 - https://doi.org/10.7868/S0015323018050108

https://doi.org/10.1134/S0031918X18050046

- 11. Gorsse S., Miracle D.B., Senkov O.N. Mapping the world of complex concentrated alloys. *Acta Materialia*. 2017;135:177–187. https://doi.org/10.1016/j.actamat.2017.06.027
- **12.** Zhang F., Zhang C., Chen S.L., Zhu J., Cao W. S., Kattner U.R. An understanding of high entropy alloys from phase diagram calculations. *Calphad*. 2014;45:1–10. https://doi.org/10.1016/j.calphad.2013.10.006
- **13.** Tsai M.-H., Yeh J.-W. High-entropy alloys: A critical review. *Materials Research Letters*. 2014;2(3):107–123. https://doi.org/10.1080/21663831.2014.912690
- **14.** Miracle D.B., Senkov O.N. A critical review of high entropy alloys and related concepts. *Acta Materialia*.

- 2017;122:448–511. https://doi.org/10.1016/j.actamat. 2016.08.081
- **15.** Miracle D.B., Miller J.D., Senkov O.N., Woodward C., Uchic M.D., Tiley J. Exploration and development of high entropy alloys for structural applications. *Entropy*. 2014;16:494–525. https://doi.org/10.3390/e16010494
- 16. Ghasemi A., Eivani A.R., Abbasi S.M., Jafarian H.R., Ghosh M., Anijdan S.H.M. Al–Co–Cr–Fe–Ni–Ti high entropy alloys: A review of microstructural and mechanical properties at elevated temperatures. *Journal of Alloys and Compounds*. 2025;1010:178216. https://doi.org/10.1016/j.jallcom.2024.178216
- 17. Zamani M.R., Mirzadeh H., Malekan M., Weißensteiner I., Roostaei M. Unveiling the strengthening mechanisms of as-cast micro-alloyed CrMnFeCoNi high-entropy alloys, *Journal of Alloys and Compounds*. 2023;957:170443. https://doi.org/10.1016/j.jallcom.2023.170443
- Nene S.S., Sinha S., Yadav D.K., Dutta A. Metallurgical aspects of high entropy alloys. *Journal of Alloys and Compounds*. 2024;1005:175849. https://doi.org/10.1016/j.jallcom.2024.175849
- Xiong W., Guo A.X.Y., Zhan S., Liu C.-T., Cao S.C. Refractory high-entropy alloys: A focused review of preparation methods and properties. *Journal of Materials Science and Technology*. 2023;142:196–215. https://doi.org/10.1016/j.jmst.2022.08.046
- Senkov O.N., Miracle D.B., Chaput K.J., Couzinie J.-P. Development and exploration of refractory high entropy alloys A review. *Journal of Materials Research*. 2018;33(19):3092–3128. https://doi.org/10.1557/jmr.2018.153
- **21.** Zheng W., Lü S., Wu S., Chen X., Guo W. Development of MoNbVTa_x refractory high entropy alloy with high strength at elevated temperature. *Materials Science and Engineering: A.* 2022;850:143554. https://doi.org/10.1016/j.msea.2022.143554
- Senkov O.N., Wilks G.B., Miracle D.B., Chuang C.P., Liaw P.K. Refractory high-entropy alloys. *Intermetallics*. 2010;18(9):1758–1765. https://doi.org/10.1016/j.intermet.2010.05.014
- 23. Senkov O.N., Wilks G.B., Scott J.M., Miracle D.B. Mechanical properties of Nb₂₅Mo₂₅Ta₂₅W₂₅ and V₂₀Nb₂₀Mo₂₀Ta₂₀W₂₀ refractory high entropy alloys. *Intermetallics*. 2011;19(5): 698–706. https://doi.org/10.1016/j.intermet.2011.01.004
- **24.** Carter T.J. Common failures in gas turbine blades. *Engineering Failure Analysis*. 2005;12(2):237–247. https://doi.org/10.1016/j.engfailanal.2004.07.004
- **25.** Tancret F., Sourmail T., Yescas M.A., Evans R.W., McAleese C., Singh L., Smeeton T., Bhadeshia H.K.D.H. Design of creep-resistant nickel-base superalloy for power plant applications. *Materials Science and Technology*. 2003;19:291–302.
- 26. Das S., Robi P.S. A novel refractory WMoVCrTa high-entropy alloy possessing fine combination of compressive stress-strain and high hardness properties. *Advanced Powder Technology*. 2020;31(12):4619–4631. https://doi.org/10.1016/j.apt.2020.10.008
- 27. Moser M., Dine S., Vrel D., Perriere L., Pires-Brazuna R., Couque H., Bernard F. Elaboration and characterization of WMoTaNb high entropy alloy prepared by powder



- metallurgy processes. Materials. 2022;15(15):5416. https://doi.org/10.3390/ma15155416
- 28. Cao Y., Liu Y., Liu B., Zhang W. Precipitation behavior during hot deformation of powder metallurgy Ti-Nb-Ta-Zr-Al high entropy alloys. *Intermetallics*. 2018;100:95–103. https://doi.org/10.1016/j.intermet.2018.06.007
- 29. Cao Y., Liu Y., Li Y., Liu B., Fu A., Nie Y. Precipitation behavior and mechanical properties of a hot-worked TiNbTa_{0.5}ZrAl_{0.5} refractory high entropy alloy. *Interna*tional Journal of Refractory Metals and Hard Materials. 2020;86:105132.
 - https://doi.org/10.1016/j.ijrmhm.2019.105132
- 30. Guo W., Liu B., Liu Y., Li T., Fu A., Fang Q., Nie Y. Microstructures and mechanical properties of ductile NbTaTiV refractory high entropy alloy prepared by powder metallurgy. Journal of Alloys and Compounds. 2019;776: 428–436. https://doi.org/10.1016/j.jallcom.2018.10.230
- 31. Dirras G., Gubicza J., Heczel A., Lilensten L., Couzinié J.-P., Perriére L., Guillot I., Hocini A. Microstructural investigation of plastically deformed Ti₂₀Zr₂₀Hf₂₀Nb₂₀Ta₂₀ high entropy alloy by X-ray diffraction and transmission electron microscopy. Materials Characterization. 2015;108:1-7.
 - https://doi.org/10.1016/j.matchar.2015.08.007
- 32. Jia Y., Wang G., Wu S., Mu Y., Yi Y., Jia Y., Liaw P.K., Zhang T., Liu C.-T. A lightweight refractory complex concentrated alloy with high strength and uniform ductility. Applied Materials Today. 2022;27:101429. https://doi.org/10.1016/J.APMT.2022.101429.
- 33. Yurchenko N., Panina E., Zherebtsov S., Stepanov N. Design and characterization of eutectic refractory high entropy alloys. Materialia. 2021;16:101057. https://doi.org/10.1016/J.MTLA.2021.101057
- 34. Stepanov N.D., Yurchenko N.Yu., Skibin D.V., Tikhonovsky M.A., Salishchev G.A., Structure and mechanical properties of the AlCr NbTiV (x = 0, 0.5, 1, 1.5) high entropy alloys. Journal of Alloys and Compounds. 2015;652:266-280.
- https://doi.org/10.1016/j.jallcom.2015.08.224
- 35. Yurchenko N., Panina E., Tikhonovsky M., Salishchev G., Zherebtsov S., Stepanov N. A new refractory Ti-Nb-Hf-Al high entropy alloy strengthened by orthorhombic phase particles. International Journal of Refractory Metals and Hard Materials. 2020;92:105322.
 - https://doi.org/10.1016/J.IJRMHM.2020.105322
- 36. Senkov O.N., Senkova S.V., Woodward C., Miracle D.B. Low-density, refractory multi-principal element alloys of the Cr-Nb-Ti-V-Zr system: Microstructure and phase analysis. Acta Materialia. 2013;61(5):1545–1557. https://doi.org/10.1016/j.actamat.2012.11.032
- 37. Senkov O.N., Senkova S.V., Miracle D.B., Woodward C. Mechanical properties of low-density, refractory multiprincipal element alloys of the Cr-Nb-Ti-V-Zr system. Journal of Materials Science and Engineering. 2013;565:51-62.
 - https://doi.org/10.1016/j.msea.2012.12.018
- 38. Ren X., Li Y., Qi Y., Wang B. Review on preparation technology and properties of refractory high entropy alloys. Materials. 2022;15(8):2931. https://doi.org/ 10.3390/ma15082931

- 39. Shojaei Z., Khayati G.R, Darezereshki E. Review of electrodeposition methods for the preparation of high-entropy alloys. International Journal of Minerals, Metallurgy and Materials. 2022;29:1683-1696. https://doi.org/10.1007/s12613-022-2439-y
- 40. Sanin V.N., Yukhvid V.I., Ikornikov D.M., Andreev D.E., Sachkova N.V., Alymov M.I. SHS metallurgy of high-entropy transition metal alloys. Doklady Physical Chemistry. 2016;470:145-149.

https://doi.org/10.1134/S001250161610002X

- Санин В.Н., Юхвид В.И., Икорников Д.М., Андреев Д.Е., Сачкова Н.В., Алымов М.И. СВС-металлургия литых высокоэнтропийных сплавов на основе переходных металлов. Доклады Академии наук. 2016;470(4):421-426.
- https://doi.org/10.7868/S0869565216280124
- 41. Sanin V.N., Ikornikov D.M., Golosova O.A., Andreev D.E., Yukhvid V.I. Centrifugal metallothermic SHS of cast Co-Cr-Fe-Ni-Mn-(X) alloys. Russian Journal of Non-Ferrous Metals. 2020;61(4):436-445. https://doi.org/10.3103/S1067821220040070
 - Санин В.Н., Икорников Д.М., Голосова О.А., Андреев Д.Е., Юхвид В.И. Центробежная СВС-металлургия легированных высокоэнтропийных литых сплавов на основе системы Со-Ст-Fe-Ni-Mn-(X). Известия вузов. Цветная металлургия. 2020;(3):59-71. https://doi.org/10.17073/0021-3438-2020-3-59-71
- 42. Sanin V.N., Ikornikov D.M., Golosova O.A., Andreev D.E., Yukhvid V.I. Centrifugal SHS metallurgy of cast Co-Cr-Fe-Ni-Mn high-entropy alloys strengthened by precipitates based on Mo and Nb borides and silicides. Physical Mesomechanics. 2021;24(6):692–700. https://doi.org/10.1134/S1029959921060072
 - Санин В.Н., Икорников Д.М., Голосова О.А., Андреев Д.Е., Санин В.В., Юхвид В.И. Центробежная СВС-металлургия литых высокоэнтропийных сплавов системы Co-Cr-Fe-Ni-Mn, упрочняемых структурными выделениями на основе боридов и силицидов Мо и Nb. Физическая мезомеханика. 2021;24(4):73-82.
 - https://doi.org/10.24412/1683-805X-2021-4-73-82
- 43. Kubanova A.N., Ikornikov D.M., Sanin V.D., Martynov D.A. Cast Mo-Cr, W-Cr, and Cr-Al master alloys by gravity-assisted SHS metallurgy. International Journal of Self-Propagating High-Temperature Synthesis. 2024;33(4):295–302. https://doi.org/10.3103/S1061386224700274
- 44. Sanin V., Andreev D., Ikornikov D., Yukhvid V. Cast intermetallic alloys and composites based on them by combined centrifugal casting - SHS process. Open Journal of Metal. 2013;3(2B):12-24. https://doi.org/10.4236/ojmetal.2013.32A2003
- 45. Martynov D.A., Sanin V.N. A centrifugal installation for the production of cast materials by centrifugal SHS-cast-

ing methods: Patent 2814351 (RF). 2024.

Мартынов Д.А., Санин В.Н. Центробежная установка для получения литых материалов методами центробежного СВС-литья: Патент 2814351 (РФ). 2024.



- **46.** Shiryaev A.A. Thermodynamic of SHS: modern approach. *International Journal of Self-Propagating High-Temperature Synthesis*. 1995;4(4):351–362.
- **47.** Shiryaev A.A. Distinctive features of thermodynamic analysis in SHS investigations. *Journal of Engineering Physics and Thermophysics*. 1993;65:957–962. https://doi.org/101007/BF00862765
 - Шариев А.А. Особенности использования метода термодинамического анализа при исследовании процессов СВС. *Инженерно-физический журнал*. 1993;65(4):412–419.
- **48.** Gorr B., Schellert S., Müller F., Christ H.J., Kauffmann A., Heilmaier M. Current status of research on the oxidation

- behavior of refractory high entropy alloys. *Advanced Engineering Materials*. 2021;23(5):2001047. https://doi.org/10.1002/adem.202001047
- **49.** Waseem O.A., Ryu H.J. Combinatorial synthesis and analysis of Al_xTa_yV_z-Cr₂₀Mo₂₀Nb₂₀Ti₂₀Zr₁₀ and Al₁₀CrMo_xNbTiZr₁₀ refractory high-entropy alloys: Oxidation behavior. *Journal of Alloys and Compounds*. 2020;828:154427. https://doi.org/10.1016/j.jallcom.2020.154427
- **50.** Yurchenko N., Panina E., Zherebtsov S., Stepanov N. Oxidation behaviour of refractory (HfCo)_{100-x}(NbMo)_x highentropy alloys with a bcc+B2 structure. *Applied Sciences*. 2023;13(16):9336.

https://doi.org/10.3390/app13169336

Information about the Authors

Vladimir N. Sanin – Dr. Sci. (Eng.), Chief Researcher of the Laboratory of liquid-phase SHS processes and cast materials of Merzhanov Institute of Structural Macrokinetics and Materials Science of the Russian Academy of Sciences (ISMAN)

(D) ORCID: 0000-0001-8402-4605

E-mail: svn@ism.ac.ru

Denis M. Ikornikov – Research Engineer, Junior Researcher of the Laboratory of liquid-phase SHS processes and cast materials, ISMAN

(D) ORCID: 0000-0002-8082-4442 **☑ E-mail**: denis-ikornikov@yandex.ru

Alina O. Sivakova – Postgraduate Student, Junior Researcher of the Laboratory of physical materials science, ISMAN

(D) *ORCID*: 0009-0000-7292-5887 **☑** *E-mail:* sivakovaalina@yandex.ru

Dmitry Yu. Kovalev – Dr. Sci. (Phys.-Math.), Head of the Laboratory of *X*-ray investigation, Chief Researcher, ISMAN

(D) ORCID: 0000-0002-8285-5656

E-mail: kovalev@ism.ac.ru

Sergey L. Silyakov – Cand. Sci. (Eng.), Senior Researcher of the Laboratory of liquid-phase SHS processes and cast materials, ISMAN

E-mail: ssl@ism.ac.ru

Milena D. Panova – Junior Researcher of the Laboratory of metallurgical processes of JSC "State Scientific Research and Design Institute of the Rare Metal Industry "Giredmet"

E-mail: MDPanova@rosatom.ru

Сведения об авторах

Владимир Николаевич Санин – д.т.н., гл. науч. сотрудник лаборатории жидкофазных СВС-процессов и литых материалов Института структурной макрокинетики и проблем материаловедения им. А.Г. Мержанова Российской академии наук (ИСМАН)

(D) ORCID: 0000-0001-8402-4605

💌 E-mail: svn@ism.ac.ru

Денис Михайлович Икорников – инженер-исследователь, мл. науч. сотрудник лаборатории жидкофазных СВС-процессов и литых материалов ИСМАН

(D) ORCID: 0000-0002-8082-4442

E-mail: denis-ikornikov@yandex.ru

Алина Олеговна Сивакова – аспирант, мл. науч. сотрудник лаборатории физического материаловедения ИСМАН

(D) ORCID: 0009-0000-7292-5887

E-mail: sivakovaalina@yandex.ru

Дмитрий Юрьевич Ковалев – д.ф-м.н., заведующий лабораторией рентгеноструктурных исследований, гл. науч. сотрудник ИСМАН

(D) ORCID: 0000-0002-8285-5656

💌 **E-mail:** kovalev@ism.ac.ru

Сергей Леонидович Силяков – к.т.н., ст. науч. сотрудник лаборатории жидкофазных СВС-процессов и литых материалов ИСМАН

E-mail: ssl@ism.ac.ru

Милена Денисовна Панова – мл. науч. сотрудник лаборатории металлургических процессов АО «Государственный научно-исследовательский и проектный институт редкометаллической промышленности «Гиредмет»

E-mail: MDPanova@rosatom.ru

Contribution of the Authors



Вклад авторов

V. N. Sanin – developed the main concept, defined the aims and objectives of the study, supervised the research, organized the work, discussed the findings, and prepared the manuscript.

D. M. Ikornikov – performed the thermodynamic analysis, conducted alloy synthesis experiments, collected and analyzed experimental data, processed the results, and contributed to manuscript preparation.

A. *O. Sivakova* – carried out microstructural analysis of the synthesized alloys, analyzed and processed the data, and contributed to manuscript preparation.

В. Н. Санин – формирование основной концепции, определение целей и задач исследования, руководство исследованием, организация работ, обсуждение результатов исследования, подготовка текста статьи.

Д. М. Икорников – термодинамический анализ, проведение исследований по синтезу сплавов, сбор и анализ экспериментальных данных, обработка результатов, подготовка текста статьи.

А. О. Сивакова – микроструктурной анализ синтезированных сплавов, анализ данных, обработка результатов, подготовка текста статьи.

POWDER METALLURGY AND FUNCTIONAL COATINGS. 2025;19(5):17-35



Sanin V.N., Ikornikov D.M., and etc. Synthesis of refractory high-entropy alloys based ...

D. Yu. Kovalev – conducted *X*-ray phase analysis of the synthesized alloys, processed and interpreted the data, and contributed to manuscript preparation.

 $\it S.\,L.\,Silyakov$ – collected and analyzed experimental data, processed the results, and prepared them for inclusion in the manuscript.

M. D. Panova – investigated the oxidation resistance of the synthesized alloys, processed and interpreted the data, and contributed to manuscript preparation.

Д. Ю. Ковалев – рентгенофазовый анализ синтезированных сплавов, аналитическая обработка полученных данных, обработка результатов, подготовка текста статьи.

С. Л. Силяков – сбор и анализ экспериментальных данных, обработка результатов и их подготовка для статьи.

М. Д. Панова – исследование окислительной стойкости синтезированных сплавов, аналитическая обработка полученных данных, обработка результатов, подготовка текста статьи.

Received 26.02.2025 Revised 15.04.2025 Accepted 17.04.2025 Статья поступила 26.02.2025 г. Доработана 15.04.2025 г. Принята к публикации 17.04.2025 г.